The Kinetics of the Reduction of Iron Oxide by Carbon Monoxide Mixed with Carbon Dioxide

C. D. Bohn
Dept of Chemical Engineering and Biotechnology, University of Cambridge, Cambridge CB2 3RA, U.K

J. P. Cleeton
Dept of Engineering, University of Cambridge, Cambridge CB2 1PZ, U.K

C. R. Müller
Dept of Chemical Engineering and Biotechnology, University of Cambridge, Cambridge CB2 3RA, U.K
Dept of Engineering, University of Cambridge, Cambridge CB2 1PZ, U.K

J. F. Davidson and A. N. Hayhurst
Dept of Chemical Engineering and Biotechnology, University of Cambridge, Cambridge CB2 3RA, U.K

S. A. Scott
Dept of Engineering, University of Cambridge, Cambridge CB2 1PZ, U.K

J. S. Dennis
Dept of Chemical Engineering and Biotechnology, University of Cambridge, Cambridge CB2 3RA, U.K

DOI 10.1002/aic.12084
Published online October 30, 2009 in Wiley InterScience (www.interscience.wiley.com).

Results are reported for the repeated reduction of iron oxide particles, 300–425 μm diameter, by a mixture of CO, CO_2, and N_2 in a fluidized bed of 20 mm internal diameter. The conclusions were as follows: (1) Reduction of either Fe_2O_3 to Fe_3O_4 or of Fe_3O_4 to $Fe_{0.947}O$ is first-order in CO. (2) With the particle sizes used, the rates of the reduction reactions are controlled by intrinsic chemical kinetics. Activation energies and pre-exponential factors are reported. (3) The first cycle gave anomalous results, but (a) the rate of reduction of Fe_2O_3 to Fe_3O_4 remained constant over cycles 2–10; (b) the rate of reduction of Fe_3O_4 to $Fe_{0.947}O$ declined by 60–85% over cycles 2–10. (4) The rates of reduction declined with solids conversion down to zero at 80% conversion. The rates were incorporated into a conventional model of a fixed bed, which was used to predict, satisfactorily, the reduction behavior of iron oxide. © 2009 American Institute of Chemical Engineers *AIChE J,* 56: 1016–1029, 2010
Keywords: reaction kinetics, iron oxide reduction, hydrogen production, fluidized bed

Introduction

The need to reduce emissions of greenhouse gases by introducing environmentally benign fuels such as H_2 is now widely accepted.[1] The reduction and oxidation reactions

Correspondence concerning this article should be addressed to C. D. Bohn at cdb36@cam.ac.uk

involving iron oxides with mixtures of either carbon monoxide and carbon dioxide and/or hydrogen and steam provide a method for converting a carbonaceous fuel, such as coal or biomass, into pure hydrogen, while simultaneously separating carbon dioxide. The species of iron and its oxides involved are Fe_2O_3, Fe_3O_4, $Fe_{1-y}O$, and Fe. Here, $0.05 < y < 0.17$ arises from vacancies in the lattice.[2] The reduction of Fe_2O_3 by CO, produced externally by for example gasification of a solid fuel, occurs via:

$$3\,Fe_2O_3 + CO \rightleftarrows 2\,Fe_3O_4 + CO_2; \quad \Delta H^{\circ}_{1023\,K} = -44.3\ \text{kJ/mol} \quad \text{(R1)}$$

$$0.947\,Fe_3O_4 + 0.788\,CO \rightleftarrows 3\,Fe_{0.947}O + 0.788\,CO_2; \quad \Delta H^{\circ}_{1023\,K} = +21.1\ \text{kJ/mol} \quad \text{(R2)}$$

$$Fe_{0.947}O + CO \rightleftarrows 0.947\,Fe + CO_2; \quad \Delta H^{\circ}_{1023\,K} = -20.3\ \text{kJ/mol} \quad \text{(R3)}$$

The equilibrium constant for (R1), $K_p = p_{co_2}/p_{co}$, is larger than 10^4 between 298 and 1400 K, implying that the presence of Fe_2O_3 will permit nearly complete conversion of the CO in a reducing gas to CO_2 in the thermodynamic limit. Similar reactions can be written for reduction with H_2, and thermodynamics again predicts complete conversion of the H_2 to H_2O in the presence of Fe_2O_3. Therefore, following condensation of the H_2O, pure CO_2 is produced at this stage which can be sequestered directly. Further reduction to $Fe_{0.947}O$ or Fe can be carried out without significant CO slip, if the reduction proceeds in a reactor which permits concentration gradients in the gaseous phase, e.g., a packed bed.

The reduced metal or metal oxide can then be reoxidised with steam in a separate stage to produce the desired hydrogen:

$$0.947\,Fe + H_2O_{(g)} \rightleftarrows Fe_{0.947}O + H_2; \quad \Delta H^{\circ}_{1023\,K} = -13.8\ \text{kJ/mol} \quad \text{(R4)}$$

$$3\,Fe_{0.947}O + 0.788\,H_2O_{(g)} \rightleftarrows 0.947\,Fe_3O_4 + 0.788\,H_2; \quad \Delta H^{\circ}_{1023\,K} = -48.0\ \text{kJ/mol} \quad \text{(R5)}$$

It has been shown by Bohn et al.[3] that the H_2 produced in this way has a CO contamination of <50 ppm, which compares with CO levels of ~0.5 vol % in the H_2 produced from conventional reforming, followed by low-temperature shift.[4] Thus, the hydrogen from this process is suitable for use in polymeric membrane fuel cells.

Finally, the Fe_3O_4 produced by (R5) is returned to its original form, Fe_2O_3, via oxidation in air:

$$2\,Fe_3O_4 + 1/2\,O_2 \rightleftarrows 3\,Fe_2O_3; \quad \Delta H^{\circ}_{1023\,K} = -238.4\ \text{kJ/mol} \quad \text{(R6)}$$

In the overall process, no iron is consumed and the net reaction starting with carbon from coal or biomass is:

$$C_{(s)} + 1.25\,H_2O_{(g)} + 0.375\,O_2 \rightleftarrows CO_2 + 1.25\,H_2; \quad \Delta H^{\circ}_{298\,K} = -90.6\ \text{kJ/mol} \quad \text{(R7)}$$

The potential of the proposed process lies in the fact that a carbonaceous fuel can be used to produce separate streams of (i) pure CO_2 and (ii) pure H_2 and also useful heat.

The steam-iron process (SIR) given by reactions (R1–R5) was patented by Messerschmidt[5] in 1910. The original concept was later modified to include interconnected fluidised beds to permit continuous operation via looping of solids.[6,7] Other metals, e.g. Cu[8] and Ni,[9] have been investigated for their ability to sequester carbon in chemical looping combustion (CLC); however, they cannot produce H_2 owing to thermodynamic constraints.

While the equilibrium constants for reactions (R1)–(R3) are well-established and derivable from standard thermodynamic data,[10,11] their intrinsic kinetics are less easily obtained. Research on the kinetics of reduction of iron oxide has stemmed from the steel industry and has been characterised by a progression towards increasingly complex rate models. Initial investigations used a single step reduction mechanism, whereby Fe_2O_3 was reduced to Fe without the intermediates Fe_3O_4 and $Fe_{0.947}O$.[12] McKewan has studied single step reduction for the case of H_2.[13,14] Later, two-step models including wuestite, $Fe_{0.947}O$, were developed.[12] A model involving all four species of iron and its oxides was then proposed by Spitzer et al.[15] for porous pellets, whose reduction in H_2 was controlled by internal transport and reaction resistances at three sharply defined shrinking cores corresponding to the boundaries, at successively decreasing radii, between Fe, $Fe_{0.947}O$, Fe_3O_4, and Fe_2O_3. Murayama et al.[16] applied this shrinking core approach to the reduction of iron oxide with mixtures of CO and CO_2. Implicit in the model is the assumption that reactions occur at sharp fronts, which holds if $\sqrt{D_e/k_i} \ll d_p$, i.e., the square root of the ratio of the effective diffusivity of the gas, D_e, to the first order rate constant, k_i, must be substantially less than the particle's diameter, d_p. This assumption holds in dense mineral iron ores, but fails in porous particles designed for repeated redox cycles in, e.g., the steam-iron process.

To address reduction with diffuse interfaces, Szekely and Evans[17] proposed a grain model where the overall pellet is comprised of dense spherical subparticles which are chemically reduced at sharp interfaces. They applied the grain model to the reduction of NiO by H_2. This model has since been applied to the reduction of iron oxide, e.g., Ref. 18. Alternatively, Trushenski et al.[19] proposed a model for reaction occurring over a specific volume of the pellet, rather than over the surface area of an interface. Both Szekely's and Trushenski's models permit diffuse interfaces and have been successfully employed to describe experimental results over broad ranges of gas composition and temperature.

In the aforementioned models, the rate parameters were obtained by fitting theoretical predictions to experimental results influenced by intra-particle gaseous diffusion, e.g., Ref. 19,20 As such, the rate constants did not have as significant an effect on the models' predictions as would be the case in a purely kinetically controlled regime. Recently, growing interest in gas-solid looping cycles, e.g., for the sequestration of CO_2, has also presented a need for the kinetics of the reduction of iron oxide to be studied over repeated cycles of reduction and oxidation, instead of just during an initial cycle.

The objectives of this present study were therefore to:

(1) determine pre-exponential factors and activation energies for the reduction of the iron oxides by mixtures of CO and CO_2 in the kinetically controlled regime at industrially relevant temperatures and pressures;

(2) measure the rates in a fluidised bed where the effects of external heat and mass transfer are minimized;

(3) investigate any changes in the kinetics after increasing numbers of cycles and

(4) compare theoretical predictions with measurements obtained in experiments different from those used to derive the kinetic parameters, e.g., by using the rate parameters obtained in a fluidised bed to predict the reduction of a fixed bed of iron oxide.

Experimental

The particles of iron oxide were prepared by spraying water from reverse osmosis on to Fe_2O_3 powder (Sigma-Aldrich; purity $>$ 99.9 wt %) while mechanically mixing. The resulting agglomerates were heated at 1173 K for 3 h and then sieved to the desired size ranges. The BET surface area of the sintered Fe_2O_3 particles with $d_p \approx$ 300–425 μm was $\sim$0.5 m^2/g (Micromeritics, Tristar 3000); the porosity, measured by Hg porosimetry (Micromeritics, Autopore IV) was 0.60. The surface area of particles of Fe_3O_4 reduced from Fe_2O_3 at 1173 K with $d_p \approx$ 300–425 μm was $\sim$0.4 m^2/g with a porosity of 0.58. The particles were added to the reactor as Fe_2O_3 and the mass of the batch was measured using a balance with a precision of 10^{-4} g (OHaus).

The fluidized bed reactor is shown in Figure 1 and consisted of a tube of recrystallised Al_2O_3 (i.d. 20 mm) with a perforated plate distributor, also of Al_2O_3; both had purities $>$ 99.9 wt %. The plate had 5 holes, each 1 mm dia., four aligned in a square array of side 8 mm, with one central hole. The tube and disc were joined using ceramic cement (ALCS, Multilab). Approximately 10 g of Al_2O_3 ($d_p \approx$ 1400–1700 μm; $\rho_{Al_2O_3} = 3770$ kg/m^3; Boud Mineral) formed a packed bed beneath the distributor, held in place with quartz wool; this packed bed pre-heated the gas entering the reactor, as shown in Figure 1. The fluidised material consisted of 15 g of Al_2O_3 (purity $>$ 99.9 wt %) sieved to $d_p \approx$ 300–425 μm. The depth of the unfluidised bed, H_0, was 30 mm, giving an aspect ratio, $H_0/d_{bed} = 1.5$. The reactor was placed in a tubular furnace, and its temperature was measured by a type K thermocouple, positioned 5 mm above the distributor, inside the bed.

Gas was supplied to the reactor from cylinders of (i) pure CO_2, (ii) 10 vol % CO or 30 vol % CO, balance N_2 and (iii) pure N_2; (iv) laboratory air was also supplied. The flowrates of streams (ii)–(iv) were measured using mass flow meters (AWM5101VN, Honeywell), but with stream (i) a rotameter was used. Steam was supplied using a syringe pump to feed liquid H_2O at a flowrate of 30 ml/h through hypodermic tubing (0.8 mm i.d.) into an electrically-heated boiler maintained at 433 K. The gas and superheated steam were mixed and then fed into the reactor via a heated line at 433 K. For all experiments, $U/U_{mf} \sim 7$ determined, for the mixture of reducing gas and Al_2O_3 bed particles, from the correlation of Wen and Yu.[21] Automatic switching between inlet gases was performed with solenoid valves.

The effluent gas was monitored by continuously withdrawing a sample at a flowrate of 0.6 m^3/h, measured at STP, through a quartz probe (5 mm i.d.) and measuring its composition by (i) nondispersive infrared, measuring [CO] and [CO_2] in the range 0–20 vol.% (ABB), (ii) nondispersive infrared measuring [CO] in the range 0–2000 vol ppm (ABB) and (iii) measuring thermal conductivity to yield [H_2] in the range 0–30 vol% (ABB). As steam was used to convert the $Fe_{0.947}O$ to Fe_3O_4, three impinger tubes immersed in an ice bath (273 K), followed by a tube filled with $CaCl_2$, were used to dry the sampled gas prior to analysis. Experiments involving cycling between Fe_2O_3 and Fe_3O_4 did not require the sampled gas to be dried. Assuming the sampling line could be modeled as a plug flow reactor in series with a well-mixed reactor, concentrations were measured with response times with and without the drying tubes, respectively, of $\tau_{CO} = 2.0$ s, $\tau_{CO_2} = 3.5$ s and $\tau_{CO} = 1.0$ s, $\tau_{CO_2} = 2.5$ s. Deconvolution did not significantly alter the results, since in all cases the total time of reaction was at least one order of magnitude greater than the listed time constants.

The transition from Fe_2O_3 to Fe_3O_4 was studied with the bed between 723 and 973 K, using mixtures of N_2+CO+CO_2 (respectively, 82, 3, and 15 vol%) during the reduction of Fe_2O_3 and mixtures of N_2+air+CO_2 (respectively, 82, 3, and 15 vol %) during oxidation of Fe_3O_4. For the transition from Fe_3O_4 to $Fe_{0.947}O$, mixtures of N_2+CO+CO_2 (respectively, 82, 9, and 9 vol %) were used to reduce Fe_3O_4 and mixtures of N_2+steam (respectively, 82 and 18 vol %) were used to oxidise $Fe_{0.947}O$ at 923–1173 K. A purge of N_2 for 60–120 s was employed between cycles to prevent mixing of the reducing and oxidising gases. Prior to any iron oxide being introduced into the reactor, one reduction and one oxidation, together constituting one cycle, were performed to ensure the inertness of the reactor, its contents, and the thermocouple in each experiment. The iron oxide particles were then poured into the reactor during a period of N_2 flow, enabling equilibration to the bed's temperature and the displacement of any air inside the iron oxide particles before reduction. The requisite reduction and oxidation cycling was then performed. The rate of reduction as a function of time was determined using the difference between the inlet and outlet concentrations of CO multiplied by the molar flowrate of fluidising gas, as described in the section on results.

The packed bed reactor was made of 316 stainless steel (i.d. 10.2 mm) and replaced the fluidised bed in some experiments. Gas was fed to the top of the reactor giving a downflow through the packed bed situated on top of a perforated plate with 7 holes, (1 mm dia.), arranged in a hexagonal arrangement with a side length of 2 mm and one central hole. The bed was loaded by placing 2 g (depth $\sim$ 12 mm) of Al_2O_3 particles with $d_p \approx$ 1400–1700 μm on top of the plate, followed by 5 g ($\sim$33 mm) of Fe_2O_3 particles with $d_p \approx$ 300–425 μm, followed by another 10 g ($\sim$60 mm) of the Al_2O_3 particles to pre-heat the gas. A type K thermocouple (o.d. 1.5 mm) placed in the interior of the reactor within the iron oxide section monitored the temperature.

Theory

In a single particle, the reduction reactions (R1) and (R2) proceed via: (i) mass transport of gaseous reactant to the exterior of the particle, (ii) diffusion of the reactant through the particle matrix, (iii) chemical reaction, (iv) diffusion of the gaseous product through the particle matrix and (v) mass transport of gaseous product into the bulk gas. Assuming (i) pseudo-steady state and (ii) first order kinetics of the form $r' \propto (c_{co} - c_{co_2}/K_p)$, a material balance over a differential volume of a single particle taking into account resistances (ii)-(iv) yields for the case of CO:

$$D_{e,CO}\left[\frac{2}{r}\frac{dc_{CO}}{dr} + \frac{d^2c_{CO}}{dr^2}\right] = k_i\left(c_{CO} - \frac{c_{CO_2}}{K_p}\right), \quad (1)$$

where c_{CO} is the concentration of CO, $D_{e,CO}$ is the effective diffusivity of CO, k_i is the intrinsic rate constant for the forward step of reaction (R1) or (R2) and r is the radial position within the particle. Substituting[22] $u_{CO} = c_{CO}r$ and employing boundary conditions of c_{CO} = constant = $c_{CO,s}$ at $r = R$ and finiteness of c_{CO} at $r = 0$ gives:

$$c_{CO}(r) = b_1 + \frac{c_1}{r}\sinh(r\sqrt{d_1}), \quad (2)$$

where $b_1 = (c_{CO_2,s} + c_{CO,s}\, D_{e,CO}/D_{e,CO_2})/(K_p + D_{e,CO}/D_{e,CO_2})$, $c_1 = Rk_i(c_{CO,s} - c_{CO_2,s}/K_p)/(c_1 D_{e,CO} d_1 \sinh(R\sqrt{d_1}))$, $d_1 = (k_i/D_{e,CO} + k_i/(K_p D_{e,CO_2}))$ and $c_{CO,s}$ and $c_{CO_2,s}$ are the concentrations at the external surface of the particle. A similar procedure can be used to solve for $c_{CO_2}(r)$.

The effectiveness factor and Thiele modulus are then given, respectively, by:

$$\eta = \frac{3}{\phi^2}(\phi\coth\phi - 1), \quad \phi = R\sqrt{\frac{k_i}{D_{e,CO}} + \frac{k_i}{K_p D_{e,CO_2}}}. \quad (3)$$

This definition is similar to that of Levenspiel,[23] except that ϕ includes the reverse reaction represented by the term containing K_p. Incorporating the resistance to mass transfer through the film layer, the specific rate of reaction, r', in mol/(s g) for a single particle can be written as:

$$\left.\begin{aligned} r' &= \frac{k}{\rho_{Fe_2O_3}}\left(c_{CO,p} - \frac{c_{CO_2,p}}{K_p}\right), \\ \frac{1}{k} &= \frac{R}{3k_{g,co}} + \frac{1}{k_i\eta} + \frac{R}{3k_{g,co_2}K_p}. \end{aligned}\right\} \quad (4)$$

Here, $c_{CO,p}$ and $c_{CO_2,p}$ are the concentrations in the particulate or bulk phase of the reactor, $\rho_{Fe_2O_3}$ is the density of the particle, $k_{g,CO}$ and k_{g,CO_2} are the mass transfer coefficients, k_i is the intrinsic rate constant for reaction (R1) or (R2) and R is the particle's external radius. Unless otherwise specified, the equilibrium constant, K_p, was determined from published thermodynamic data.[10]

The bubble to particulate phase resistance of the fluidised bed could be incorporated using the two-phase model of Davidson and Harrison.[24] However, by measuring the rate of reaction, when increasing masses of iron oxide were added to the bed, a crossflow factor[24] greater than 2.5 was determined for all experiments. The particles of Al_2O_3 and iron oxide were also of similar size and density such that no segregation was observed. The absence of segregation, and the high crossflow factor, imply that the bed behaves like a CSTR in respect of both the gas and particulate phases. Hence, the final rate expression used to analyze the reduction of Fe_2O_3 particles with particle density, $\rho_{Fe_2O_3}$, is expressed in units of mol/(s g) as:

$$r' = \frac{k}{\rho_{Fe_2O_3}}\left(c_{CO,out} - \frac{c_{CO_2,out}}{K_p}\right), \quad (5)$$

Here, the mass transfer coefficients, $k_{g,CO}$ and k_{g,CO_2}, for one particle were estimated from $Sh = 2\varepsilon_{mf} + 0.69Re_p^{1/2}Sc^{1/3}$, similar to La Nauze,[25] where $Sh = k_g d_p/D_{mix}$ with $\varepsilon_{mf} = 0.45$. The effective diffusivity of CO or CO_2 in Eqs. 1–3 was calculated from $D_e = \varepsilon/\tau(1/D_k + 1/D_{mix})^{-1}$ using either values for CO or for CO_2. Values for the diffusion coefficients, D_{mix}, were taken from Hirschfelder et al.[26] The Knudsen diffusivity was calculated[27] using $D_k = 1.94(\varepsilon/S_g\rho_{Fe_2O_3})(T/M_w)^{1/2}m^2/s$, where $\varepsilon = 0.6$ is the porosity for Fe_2O_3 and Fe_3O_4; τ was a fitted tortuosity, found to be 3.0 and 3.5 for Fe_2O_3 and Fe_3O_4, respectively; $\rho_{Fe_2O_3} = 2060$ kg/m^3 and $\rho_{Fe_3O_4} = 2320$ kg/m^3; T is the absolute temperature; $S_g = 0.5$ m^2/g is the specific surface area for Fe_2O_3 and Fe_3O_4 and M_w is the molecular weight of the gaseous species. The influence of Knudsen diffusion on the overall effective diffusivity, D_e, was found to be minimal for both CO and CO_2.

Results

Transition from Fe_2O_3 *to* Fe_3O_4

The reduction of Fe_2O_3 to Fe_3O_4 was studied between 723 and 973 K with inlet mole fractions of CO and CO_2 set in the range from 1.5 to 2.5 vol.% and 14 to 16 vol %, respectively. Figure 2a shows the effluent mole fractions of CO and CO_2 for a typical experiment at 823 K. Here, 0.5 g of Fe_2O_3 particles with $R \sim 180$ μm were introduced into the hot bed when fluidised by N_2. After the first reduction and oxidation, the fluidizing gas was suddenly switched from N_2 to a mixture of CO, CO_2 and N_2 at $t = 30$ s. A fraction of the entering CO reacted with the Fe_2O_3 to form Fe_3O_4 and was thereby converted to CO_2. From stoichiometry, the production of CO_2 must be commensurate with the consumption of CO, and Figure 2a shows that the CO and CO_2 curves are indeed complementary. Upon completion of the reaction at $t = 100$ s, the CO and CO_2 mole fractions returned to their inlet values of 2.2 vol % and 14.8 vol %, respectively. Following a period of purging with N_2, the particles were then reoxidised with a mixture of N_2+air before undergoing subsequent reduction cycles. X-ray diffraction (Philips model PW1830/00, Cu Kα, 40 kV and 40 mA, scanning rate 0.05 degrees s^{-1}, in air at 298 K) of the reduced iron oxide confirmed the presence of Fe_3O_4. The instrument and scan sequence could detect species in excess of approximately 5 mol%; no other iron species or crystalline contaminant was found.

The conversion of the solid at a specific time can be calculated by integrating a plot (against time) of the decrease in [CO], and, or, increase in [CO_2]. The grey area in Figure 2a,

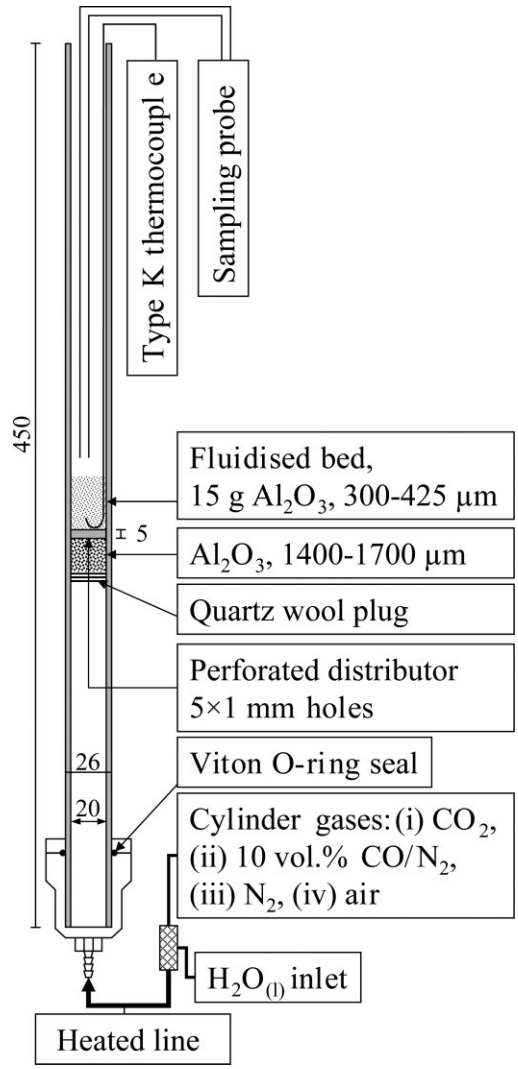

Figure 1. Schematic diagram of the fluidised bed reactor.

The inert bed material was 30 g of Al_2O_3 with $d_p \approx 300$–425 μm; active iron oxide, Fe_2O_3, in various size ranges was added to the top of the bed. All dimensions are in mm.

for example, corresponds to a conversion of 0.43 for reduction of Fe_2O_3 to Fe_3O_4. The rate at this specific conversion was then obtained by taking the instantaneous difference between the inlet and outlet mole fractions of CO or CO_2, depicted by the grey circles in Figure 2a, multiplying by the molar flowrate, and dividing by the mass of particles added: this gave the rate of reaction, r', moles/(s g). Thus, from the graph in Figure 2a a plot of rate versus conversion can be constructed and is shown in Figure 2b. The point corresponding to the rate at $X = 0.43$ is shown by the grey circle in Figure 2b. Good agreement between the rates calculated using the [CO] and [CO_2] signals is observed, although the reduced noise in the [CO] signal makes it preferable for determining the rate.

The initial rate, or rate at $X = 0$, can be derived from either Figure 2a or Figure 2b. In Figure 2a, the effluent mole fraction of CO can be approximated by a linear fit shown by the gray line and extrapolated back to the point of the gas switch. This method gives $r' = 5.3 \times 10^{-5}$ mol/(s g). In Figure 2b, the initial rate can be calculated by a linear fit of r' versus X in the interval $0.1 < X < 0.7$. The intercept of the best fit line then gives the rate at $X = 0$, shown by point A. This method gives, $r' = 4.8 \times 10^{-5}$ mol/(s g), which is in agreement to within 10% of that found from Figure 2a. For consistency, the rates reported hereinafter were determined from the plots of r' versus X. In each experiment, prior to the introduction of any iron oxide, the reducing gas was switched on and a step change in outlet concentration of CO resulted. This confirmed that the CO reacted only with the iron oxide and that the thermocouple, bed material and reactor were inert. Rates for the first reduction cycle are not reported, as it was found that the plots of [CO] and [CO_2] in the effluent were markedly different from those for cycles 2 to 10, perhaps owing to a morphological change or the presence of adsorbed gaseous species in cycle one. The anomalous behaviour during the first cycle remains puzzling and highlights the importance of investigating the rate over repeated cycles. To prevent all the inlet CO from being consumed at higher temperatures, the mass of Fe_2O_3 added to the bed was decreased progressively with temperature from 2.0 g at 623 K to 0.1 g at 973 K.

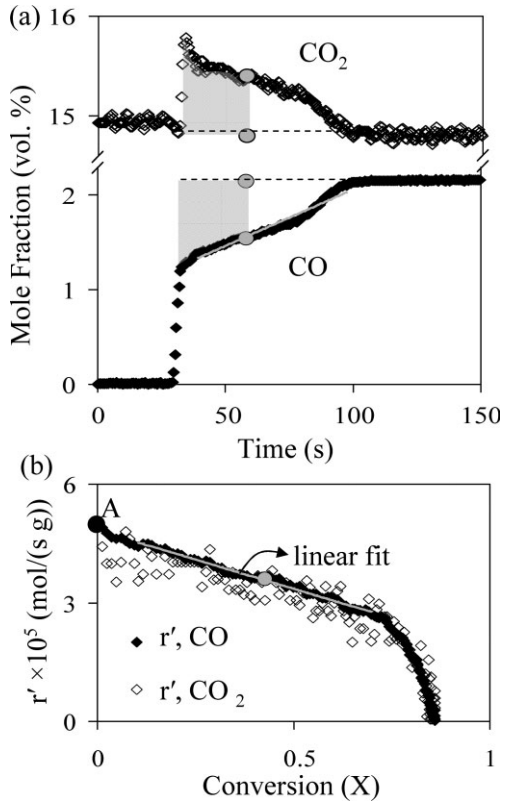

Figure 2. (a) Mole fraction of CO (◆) and CO_2 (◇) in the effluent gas versus time for the reduction of 0.5 g of Fe_2O_3 to Fe_3O_4 at 823 K. (b) Rate versus conversion calculated from the CO (◆) and CO_2 (◇) analyzer signals in (a).

The initial rate is given by the intersection of the fitted line with the ordinate at $X = 0$, shown by point A.

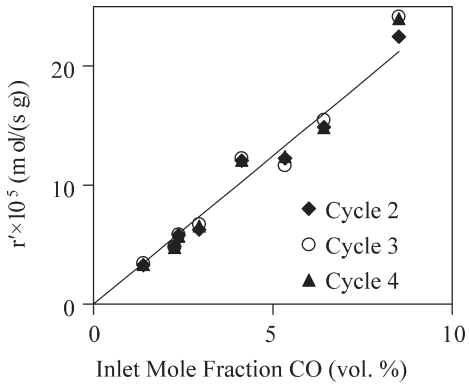

Figure 3. Reduction of Fe_2O_3 to Fe_3O_4 at 823 K.

Initial measured rate, r', at $X = 0$ versus inlet mole fraction of CO. The straight line through the origin is a best fit to the data, exhibiting a first order dependence on [CO]. The inlet mole fraction of CO_2 was fixed at 15 vol %.

The previous analysis assumed that the rate was first order in the outlet concentrations of CO and CO_2, i.e., $r' \propto (c_{\mathrm{co,out}} - c_{\mathrm{CO_2,out}}/K_{\mathrm{p}})$ in Eq. 5. Envisaging the reactor as a well-mixed CSTR and using material balances enables one to replace $c_{\mathrm{CO,out}}$ and $c_{\mathrm{CO_2},out}$ with expressions of $c_{\mathrm{CO,in}}$, $c_{\mathrm{CO_2},in}$ and r', giving $r' \propto (c_{\mathrm{co,in}} - c_{\mathrm{CO_2,in}}/K_{\mathrm{p}})$. This expression is useful since the inlet concentrations were easily measurable and controllable. By fixing the inlet mole fraction of CO_2 at 9 vol % and varying the inlet mole fraction of CO between 0 and 10 vol %, the dependence of the rate on the inlet [CO] was investigated. Figure 3 shows a plot of r' versus the mole fraction of CO in the inlet gas; the mass of Fe_2O_3 added ranged from 0.3 to 0.8 g with smaller masses used for higher mole fractions of CO. From Figure 3, the rate can be satisfactorily described by a first order fit. The dependence on [CO_2] could not be measured, since the large equilibrium constant, $K_{\mathrm{p}} = 1.47 \times 10^5$, overwhelms any effect of CO_2. The back reaction is therefore negligible here.

To determine whether the reduction of particles of Fe_2O_3 to Fe_3O_4 was limited by intrinsic kinetics or intraparticle diffusion, the rate was investigated for particles of varying radii at 823 K, fixed inlet mole fractions of CO and CO_2 of 2.5 vol % and 15 vol %, respectively, and a fixed batch mass of 0.5 g of Fe_2O_3. The observed rate constant, k, was found by dividing the rate, r', by the concentration driving force and multiplying by the bulk density, see Eq. 5. The initial intrinsic rate constant, k_0, was obtained by iteratively solving for η using Eqs. 3 and 5. For example, starting with Eq. 5 and assuming $\eta = 1$, an initial estimate of k_0 was determined. This k_0 was then used in Eq. 3 to obtain an estimate for ϕ, which was subsequently used in Eq. 3 to find a new value for η. This new value for η was then inserted into Eq. 5 to generate a new estimate of k_0. The outlined procedure was then iterated until η converged to a single value. Here, the value of the tortuosity used in the determination of the effective diffusivities was used as a fitting parameter and chosen to be $\tau = 3.0$. This value is typical of commercial pellets.[27] Figure 4a shows the observed initial rate constant, k, plotted versus particle radius, R. For $R < 300$ μm, k remains approximately constant at 490 s^{-1}. As R increases, k decreases; this pattern holds for the three reduction cycles investigated. Figure 4a also shows the initial intrinsic rate constant, k_0, for cycle 2. Applying the effectiveness factor correction has little effect on the rate constant for particles with $R < 300$ μm, since here $k = k_0$, implying $\eta = 1$. For larger particles, however, the correct value of $k_0 = 490$ s^{-1} can be recovered from the values of k. Plotting $\eta = k/490$ s^{-1} versus the calculated ϕ from Eq. 3 for each point, Figure 4b confirms that $\eta \sim 1$ for $R < 300$ μm. Also, it can be seen that for the largest particles η approaches $3/\phi$. This region corresponds to where intraparticle diffusion dominates the observed reaction rate. The size range of the particles which can be used for a kinetic study was therefore bounded by the transition to internal diffusion control at R greater than about 300 μm and the experimental observation of elutriation for R less than about 100 μm. Therefore, particles with $150\ \mu m < R < 210\ \mu m$ were used to determine the rate constants in subsequent experiments. Here, an order of magnitude estimate of the Biot number ($hd_{\mathrm{p}}/6\lambda$) for a single particle with $R \sim 180$ μm gave $Bi \ll 1$ and typically, $Bi \approx 0.03$, indicating that the temperature across a single particle was uniform. Next, a simple heat balance was used to estimate the maximum temperature difference between the particle and the bed during reduction. The temperature in the particle was assumed uniform since $Bi \ll 1$, the rate was assumed equal to the initial rate at $X = 0$; a conservative estimate of the heat transfer coefficient was obtained using

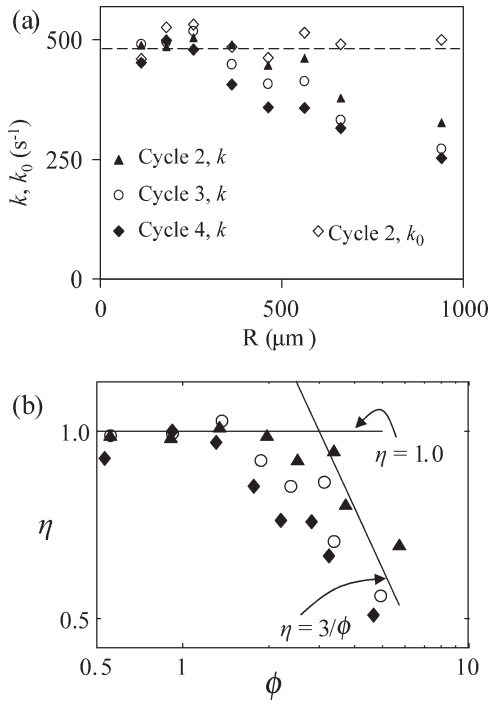

Figure 4. Reduction of 0.5 g of Fe_2O_3 to Fe_3O_4 at 823 K.

(a) Plot of initial rate constant k at $X = 0$ versus average radius, R, of the iron oxide particles for cycles 2 (▲), 3 (○) and 4 (◆). The corrected intrinsic rate constant at zero conversion, k_0, which accounts for $\eta < 1$ is also shown for cycle 2 (◇) and has an average value given by the dashed line of 490 s^{-1}. (b) Effectiveness factor, $\eta = k/490$ s^{-1}, versus calculated ϕ from Eq. 3 for cycles 2 (▲), 3 (○) and 4 (◆), corresponding to the points in (a). For smaller particles $\eta = 1.0$; as particle size increases η approaches $3/\phi$.

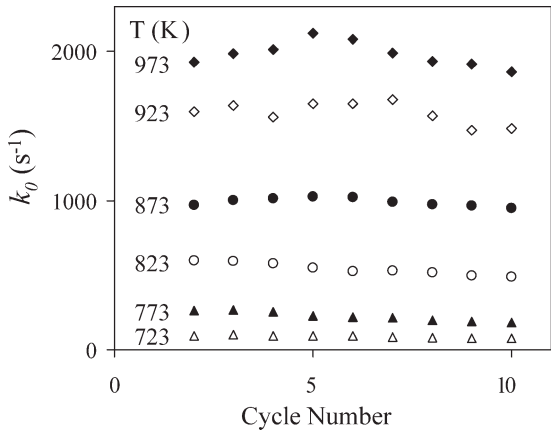

Figure 5. Initial rate constant, k_0, at zero conversion over multiple cycles of reduction and temperatures of 723 K (△), 773 K (▲), 823 K (○), 873 K (●), 923 K (◇), and 973 K (◆) for the reduction of Fe_2O_3 to Fe_3O_4.

Here, k_0 increases with temperature and remains approximately constant over multiple cycles.

$Nu = 2$ and the thermal conductivity of the reactant gas. In a fluidized bed, the true value of Nu will be larger owing to the constant contacting of new bed particles with the surface of the reacting iron particle. The maximum temperature difference between the reacting particle and the surrounding bed was found to be <10 K for all cases. Thus, it is reasonable to conclude that the temperature within a particle was the same as that of the bed.

From Figure 5, it can be observed that the initial rate constant at zero conversion increases monotonically with temperature and remains approximately constant from cycle 2 to cycle 10. The rate constant initially increases with cycle number in experiments above 873 K.

The initial rate constant was assumed to be of Arrhenius form with $k_0 = A \exp(-E/RT)$, where A is the pre-exponential factor, E the activation energy, R the gas constant and T the absolute temperature. The plot of $\ln(k_0)$ versus $10^3/(RT)$ is shown in Figure 6 and was used to determine the activation energy for particles with $R \sim 180$ μm. The activation energy was found to be $E = 72 \pm 12$ kJ/mol, 76 ± 9 kJ/mol and 78 ± 11 kJ/mol for cycles 2, 3, and 4, respectively. The activation energy was approximately constant over nine cycles with an average of $E = 75 \pm 11$ kJ/mol. The pre-exponential factor from the intercept of the best fit line with the ordinate at $10^3/RT = 0$, was determined as $\ln(A) = 17.0 \pm 1.6$, giving $A = 2.4 \times 10^7$ s^{-1}. The experimental error is reported as an error in both the activation energy and pre-exponential factor using the standard error for the line's slope and intercept, respectively, multiplied by the t -statistic for a 90% confidence interval with $(m - 2)$ degrees of freedom, where m is the number of experimental points. The errors in the activation energy and pre-exponential factor should not be combined, since they were derived from a single error in k_0 and such a combination would lead to inflated error estimates for k_0. Also shown in Figure 6 is the activation energy obtained from k for particles with $R \sim 940$ μm. For all particles shown in Figure 6, external mass transfer is negligible, so $k = \eta k_i$. It has already been shown in Figure 4 that for the 940 μm particles the effectiveness factor is approximated by $\eta = 3/\phi$; combining this with $k = \eta k_i$ gives $k = 3k_i/\phi$ and using the relation $\phi \propto k_i^{\frac{1}{2}}$ from Eq. 3 gives $k \propto k_i^{\frac{1}{2}}$. This relation demonstrates that the activation energy of the larger particles should be approximately one half that for the particles controlled by intrinsic kinetics, assuming the effective diffusivity does not change appreciably with temperature. Figure 6 shows that the activation energy for the particles with $R \sim 940$ μm is 48 ± 12 kJ/mol, which overlaps with half the value of $E = 75 \pm 11$ kJ/mol for particles with $R \sim 180$ μm.

To model the chemical reactions, the variation of r' with the conversion of Fe_2O_3 is critical. Figure 7 is a plot of k_i versus X for cycle 2 at six different temperatures. Higher values of k_i were found for higher temperatures when $X < 0.5$. For all temperatures, k_i reaches zero at $X \approx 0.8$. As conversion does not reach unity, some of the material that is weighed never reacts. The variation of k_i can be quantified by fitting $k_0 f(X) = k_0(1 - X/0.8)^a$ to the experimental points in Figure 12. This choice of $f(X)$ is the simplest function which satisfies the constraints of $f(X)_{X=0} = 1$ and $f(X)_{X=0.8} = 0$. A least squares analysis gave $a = 0.4$ and the resulting fits are shown by the solid lines in Figure 7. The rate of reduction of Fe_2O_3 to Fe_3O_4 as a function of temperature and conversion over repeated cycles of reduction can finally be summarized as

$$r' = \frac{2.4 \times 10^7 \exp\left(\frac{-75000}{RT}\right)}{\rho_{Fe_2O_3}} \left(c_{CO} - \frac{c_{CO_2}}{K_p}\right) \left(1 - \frac{X}{0.8}\right)^{0.4}. \quad (6)$$

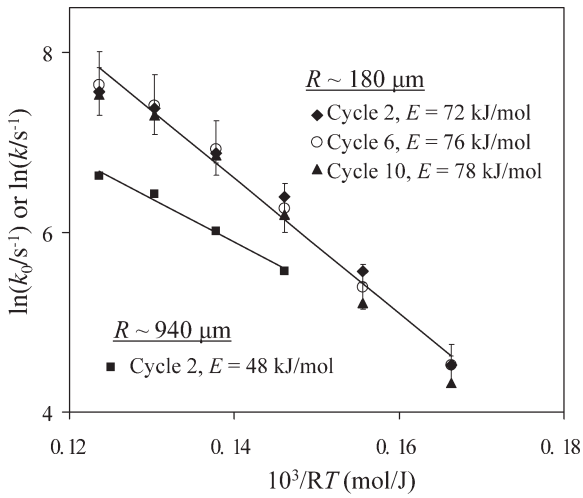

Figure 6. Arrhenius plot showing the activation energy, E, based on the initial rate constant, k_0, for the reduction of Fe_2O_3 to Fe_3O_4 for cycles 2, 6, and 10 for particles with $R \sim 180$ μm.

The average value was $E = 75$ kJ/mol. The E calculated from k for particles with $R \sim 940$ μm, where intraparticle diffusion is rate-limiting, was slightly greater than 1/2 that of particles with $R \sim 180$ μm, where intrinsic kinetics were rate-limiting.

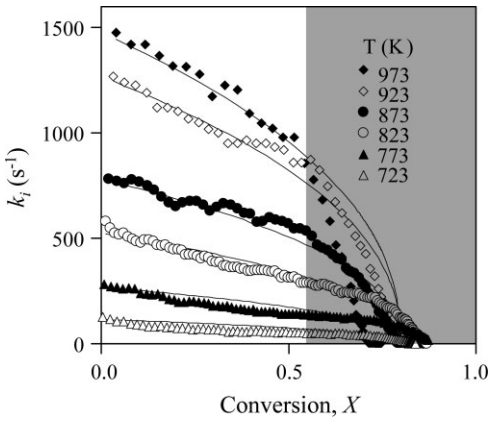

Figure 7. Plot of rate constant, k_i, against conversion, X, for cycle 2 at various temperatures.

For $X > 0.54$, k_i begins to descend to zero and the monotonic increase of k_i with temperature is lost. The solid lines represent the fit, $k_0(1 - X/0.8)^{0.4}$. The maximum conversion of $X = 0.8$ indicates that some of the weighed Fe_2O_3 never reacts.

Transition from Fe_3O_4 *to* $Fe_{0.947}O$

The reduction of Fe_3O_4 to $Fe_{0.947}O$ was studied between 923 K and 1173 K with inlet mole fractions of CO and CO_2 both set between 8.5 and 9.5 vol %. The rate at various conversions was determined from the corresponding plots of r' versus X. The mass of particles added to the bed varied between 2.2 g at 923 K and 0.4 g at 1173 K. X-ray diffraction confirmed the presence of wuestite; no other iron species was detected.

Before attempting to determine the activation energy and pre-exponential factor, the assumption that the reaction is first order with respect to CO was investigated at 1023 K with a fixed batch mass of 0.8 g of Fe_2O_3. Using material balances and assuming the bed behaves as a CSTR, the rate given by Eq. 5 as $r' \propto (c_{co,out} - c_{CO_2,out}/K_p)$ can be expressed in terms of the inlet concentrations so that $r' \propto (c_{co,in} - c_{CO_2,in}/K_p)$. Figure 8a shows the observed initial rate at $X = 0$ obtained by holding the inlet $[CO_2]$ constant at 9 vol % and varying the inlet [CO]. The rate can be described satisfactorily by a linear fit, indicating that the reaction is indeed first order with respect to [CO]. The circles on the abscissa in Figure 8a indicate the thermodynamic equilibrium points at the boundary between phases Fe_3O_4 and $Fe_{0.947}O$ (i) and $Fe_{0.947}$ O and Fe (ii), calculated from thermodynamic tables.[10] The intersection of the linear fit line in Figure 8a with the abscissa gives an experimental value of $K_p = 1.7$ for the transition from Fe_3O_4 to $Fe_{0.947}O$, found by dividing the inlet CO_2 value of 9 vol % by the CO intercept value of 5.2 vol %.

Figure 8b shows the observed initial rate at $X = 0$ obtained by holding the inlet [CO] constant at 9 vol.%, but varying the inlet $[CO_2]$. The rate varies linearly with the inlet concentration of CO_2. The circles in Figure 8b represent the thermodynamic boundaries between phases Fe_3O_4 and $Fe_{0.947}O$ (i) and $Fe_{0.947}O$ and Fe (ii) calculated from thermodynamic tables.[10] Here, the intersection of the solid fit line with the abscissa gave $[CO_2] = 18$ vol% and $K_p = 2.1$ for the equilibrium between phases Fe_3O_4 and $Fe_{0.947}O$. The theoretical calculated equilibrium value[10] of 1.87, therefore lies between the experimentally determined values of 1.7 and 2.1 for the transition from Fe_3O_4 and $Fe_{0.947}O$ at 1023 K.

To determine the regime where intrinsic kinetics solely control the observed rate, the initial rate at $X = 0$ was measured at a fixed temperature of 1023 K and fixed batch mass of 0.8 g of Fe_2O_3, whilst varying the size of the particles. The observed initial rate constant, k, is related to the true initial rate constant, k_0, by $k = k_0\eta$. Figure 9a plots k as a function of particle radius, R, over three cycles. As the particle size increases, k falls roughly proportionally to $1/R$. For particles with $R < 300$ μm, k is approximately constant at 640 s^{-1}. The true initial rate constant at zero conversion, $k_0 = 640$ s^{-1}, was found by iteratively solving for k_0 and η using Eqs. 3 and 5 as previously outlined. The resulting values for k_0 are shown in Figure 9 for cycle 2. Applying the iterative effectiveness factor correction has little effect on the rate constant for particles with $R < 300$ μm, since k

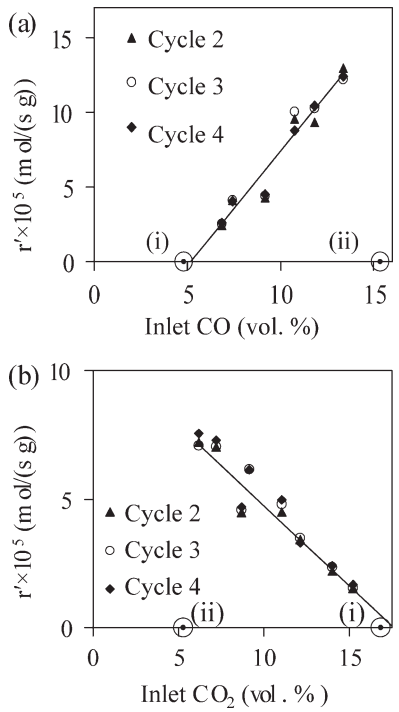

Figure 8. (a) The reaction order for [CO] for the reduction of Fe_3O_4 to $Fe_{0.947}O$ at 1023 K. The inlet mole fraction of CO_2 was held constant at ~9 vol %, and a first order fit is satisfactory.

The circles on the abscissa show thermodynamic equilibrium of (i) 9 vol % CO_2 and 4.8 vol % CO with a mixture of Fe_3O_4 and $Fe_{0.947}O$ and (ii) 9 vol % CO_2 and 15.4 vol% CO with $Fe_{0.947}O$ and Fe. (b) Relation between reaction rate and $[CO_2]$ for the reduction of Fe_3O_4 to $Fe_{0.947}O$ at 1023 K. Here, the inlet mole fraction of CO was maintained at ~9 vol %. The rate varies linearly with inlet $[CO_2]$. The circles on the abscissa show thermodynamic equilibrium of (i) thermodynamic equilibrium of a 16.8 vol % mixture of CO_2 and 9 vol% mixture of CO with Fe_3O_4 and $Fe_{0.947}O$ and (ii) 5.3 vol % CO_2 and 9 vol % CO with a mixture of $Fe_{0.947}O$ and Fe.

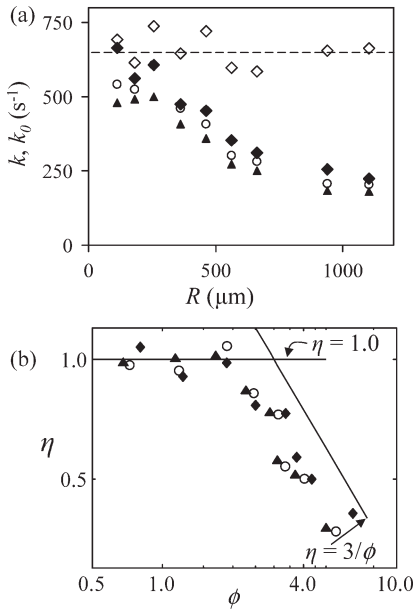

Figure 9. Reduction of Fe_3O_4 to $Fe_{0.947}O$ at 1023 K.

(a) Plot of initial rate constant k at $X = 0$ versus average radius, R, of the iron oxide particles for cycles 2 (◆), 3 (○), and 4 (▲). The corrected intrinsic rate constant at zero conversion, k_0, is also shown for cycle 2 (◇) and has an average value of 640 s^{-1}. (b) Effectiveness factor, $\eta = k/640$ s^{-1}, versus ϕ for particles of various radii for cycles 2 (◆), 3 (○) and 4 (▲), corresponding to the points in (a). For smaller particles, $\eta = 1.0$; as particle size increases η approaches $3/\phi$.

$= k_0$. Here, the tortuosity, τ, was used as a fitting parameter and set to 3.5, which is typical of porous pellets.[27] Figure 9b shows an approximation for the effectiveness factor, $\eta = k/640$ versus the calculated value of ϕ from Eq. 3 over three cycles. For particles with $R < 300$ μm, $\eta \sim 1$ indicating that the observed rate is limited by intrinsic kinetics. For larger particles, η approaches $3/\phi$, indicating that the rate is governed by intraparticle diffusion. Therefore, to avoid elutriation whilst still capturing the intrinsic kinetics, particles with $150\ \mu m < R < 210\ \mu m$ were used in all subsequent experiments. An order of magnitude estimate of the Bi number for a single particle with $R \sim 180$ μm gave $Bi \ll 1$ and typically, $Bi \approx 0.04$, indicating that the temperature across a single particle was uniform. Next, a simple heat balance was used to estimate the maximum temperature difference between the particle and the bed during reduction. The temperature in the particle was assumed uniform since $Bi \ll 1$, the rate was assumed equal to the initial rate at $X = 0$; a conservative estimate of the heat transfer coefficient was obtained using $Nu = 2$ and the thermal conductivity of the reactant gas. The maximum temperature difference between the reacting particle and the surrounding bed was found to be <6 K for all cases. Thus, it is reasonable to conclude that the temperature within a particle was the same as that of the bed.

Previously, to determine the reaction order and the regime where intrinsic kinetics dominate the reduction of Fe_2O_3 to Fe_3O_4, the initial rate at $X = 0$ was used. For determining the pre-exponential factor and activation energy for the reduction of Fe_3O_4 to $Fe_{0.947}O$, however, better precision in the value of the rate constant, k_i, can be achieved by using rates evaluated at $X > 0$. The reason derives from the first equation in Eq. 5 for k_i, which gives $k_i \propto r'/(c_{co,out} - c_{CO_2,out}/K_p)$ for negligible mass transfer resistance. For large rates, fast kinetics permit nearly complete conversion of CO to the equilibrium limit. The evaluation of the rate constant, k_i, therefore relies on division by a concentration term of small magnitude. Using smaller rates, i.e., at $X > 0$, reduces the uncertainty in k_i introduced by this term. The rate constant determined for $X > 0$ is then no longer the initial intrinsic rate constant, k_0, but is the intrinsic rate constant, k_i, at a specific conversion X.

Figure 10 shows k_i evaluated at $X = 0.3$ over nine cycles and temperatures from 923 K and 1173 K. The inlet [CO] and [CO_2] were both fixed at 9 vol % for all cases. Unlike the rate constant for the transition from Fe_2O_3 to Fe_3O_4, which remained approximately constant with cycle number, k_i decreases with cycle number. The drop in k_i is more pronounced at higher temperatures.

The rate constant was assumed to be of Arrhenius form with $k_i = A \exp(-E/RT)$. A plot of $\ln(k_i)$ versus $10^3/RT$ is shown in Figure 11. From Figure 11, the activation energy decreased slightly with cycle number for particles with $R \sim 180$ μm, ranging from $E = 106 \pm 28$ kJ/mol for cycle 2 to $E = 91 \pm 14$ kJ/mol for cycle 10. The average activation energy for the transition can be summarized by $E = 94 \pm 25$ kJ/mol. As E decreases slightly with cycle number, the decrease in the observed rate highlighted previously in Figure 10 must be a result of a decrease in the pre-exponential factor. The intercepts of the lines in Figure 11 with the ordinate, $10^3/RT = 0$, give the pre-exponential factors for a fixed conversion of $X = 0.3$. If the average value, $E = 94$ kJ/mol, is used for all cycles, the best fit lines yield $\ln(A) = 17.0 \pm 2.1$, 16.5 ± 1.9 and 15.8 ± 1.8, for cycles 2, 6, and 10, respectively, giving corresponding values of $A = 2.4 \times 10^7$, 1.5×10^7 and 7.3×10^6 s^{-1}. Figure 11 also shows that for particles with $R \sim 940$ μm the experimental activation energy calculated from k is $E = 44$ kJ/mol. The predicted activation energy from an effectiveness factor argument is one half of the E determined with particles of $R \sim 180$ μm, giving $94/2 = 47$ kJ/mol. The agreement of these values is satisfactory and suggests that the rate of reduction for the smaller particles is controlled by intrinsic kinetics, whereas

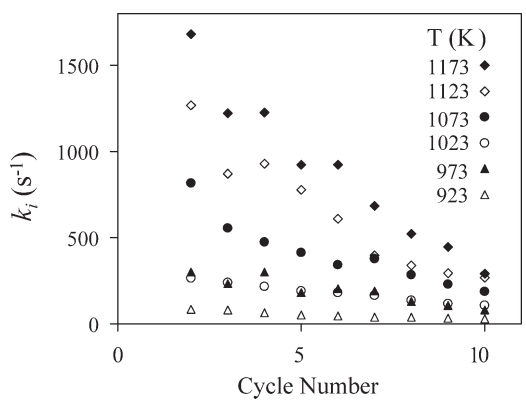

Figure 10. Intrinsic rate constant, k_i, at $X = 0.3$ for the reduction of Fe_3O_4 to $Fe_{0.947}O$.

Here, k_i increases with temperature, but decreases with the number of cycles.

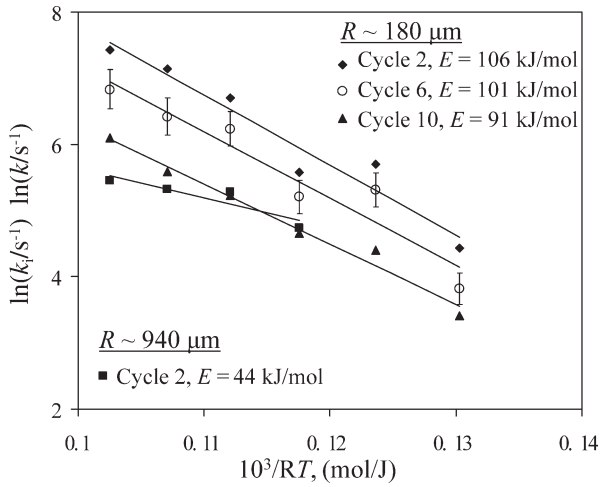

Figure 11. Activation energy diagram for the reduction of Fe_3O_4 to $Fe_{0.947}O$.

A slight decrease in E with cycle number is observed. The E from k for particles with $R \sim 940$ μm is half that observed for particles with $R \sim 180$ μm.

that for the larger particles is influenced by intraparticle diffusion.

To model the reduction of Fe_3O_4 to $Fe_{0.947}O$, the variation of the rate, r', with conversion, X must be determined. Figure 12 is a plot of k_i against X. For values of $X > 0.6$ the monotonic increase in k_i with temperature is lost; for values of $X < 0.2$, k_i increases rapidly: the rate of reaction was too fast to obtain results for $X < 0.2$ above 1023 K. The range of conversions where values of k_i could reasonably be obtained was $0.2 < X < 0.6$. In this range, values for E agreed well with those reported previously for $X = 0.3$. A least squares fit with the functional form $k_i = k_0(1 - X/0.8)^a$ gave $a = 1.2$. The fit was performed such that the correct value of k_i at $X = 0.3$ was recovered. The pre-exponential factor, A, for the initial rate constant, k_0, could then be obtained from the previously reported values of A for k_i by adding $-1.2 \ln(1-0.3/0.8) \sim 0.55$ to $\ln(A)$. Hence, the pre-exponential factors for k_0 are $\ln(A) = 17.6 \pm 2.1$, 17.1 ± 1.9 and 16.3 ± 1.8 for cycles 2, 6, and 10 respectively. These values correspond to $A = 4.3 \times 10^7$, 2.5×10^7 and 1.2×10^7 s^{-1}. Thus, the rate constants as a function of temperature and conversion for the reduction of Fe_3O_4 to $Fe_{0.947}O$ for cycles 2, 6, and 10 can be summarized by:

$$\left.\begin{aligned} r' &= \frac{4.3\times10^7 \exp\left(\frac{-94000}{RT}\right)}{\rho_{Fe_2O_3}}\left(c_{CO} - \frac{c_{CO_2}}{K_p}\right)\left(1-\frac{X}{0.8}\right)^{1.2} \\ r' &= \frac{2.5\times10^7 \exp\left(\frac{-94000}{RT}\right)}{\rho_{Fe_2O_3}}\left(c_{CO} - \frac{c_{CO_2}}{K_p}\right)\left(1-\frac{X}{0.8}\right)^{1.2} \\ r' &= \frac{1.2\times10^7 \exp\left(\frac{-94000}{RT}\right)}{\rho_{Fe_2O_3}}\left(c_{CO} - \frac{c_{CO_2}}{K_p}\right)\left(1-\frac{X}{0.8}\right)^{1.2}. \end{aligned}\right\} \quad (7)$$

where r' again has units of mol/(s g) of original particle, i.e. Fe_2O_3.

Packed bed

To verify the reported kinetic parameters, the reduction of iron oxide was investigated in a packed bed at 1023 K. A simplified model of a packed bed, which used the rate constants determined from the fluidised bed experiments given in Eqs. 6 and 7, was constructed to compare experimental results with theory. To formulate a mathematical description of the system, it was assumed that (i) the bed was isothermal, (ii) only axial concentration gradients were significant, i.e., the problem was treated as one-dimensional, (iii) the reaction rate was limited only by intrinsic kinetics and external mass transfer, not intraparticle diffusion, (iv) the dispersion coefficient was constant for both CO and CO_2 along the bed, (v) gas flowed through the interstices only, not through the porous particles. The evolution of the gaseous and metallic species in the bed as a function of time, t, and position, x are given for, e.g., CO and Fe_2O_3 by:

$$\left(\frac{\partial c_{CO}}{\partial t}\right)_x = -v\left(\frac{\partial c_{CO}}{\partial x}\right)_t + D\left(\frac{\partial^2 c_{CO}}{\partial x^2}\right)_t - \frac{(1-\varepsilon_{bed})}{\varepsilon_{bed}} \left[\underbrace{k\left(c_{CO} - \frac{c_{CO_2}}{K_p}\right)\left(1-\frac{X}{0.8}\right)^{0.4}}_{R1} + \underbrace{k\left(c_{CO} - \frac{c_{CO_2}}{K_p}\right)\left(1-\frac{X}{0.8}\right)^{1.2}}_{R2}\right] \quad (8)$$

$$A_s\left(\frac{\partial n_{Fe_2O_3}}{\partial t}\right)_x = -3A_s(1-\varepsilon_{bed})\underbrace{k\left(c_{CO} - \frac{c_{CO_2}}{K_p}\right)\left(1-\frac{X}{0.8}\right)^{0.4}}_{R1}, \quad (9)$$

where the parameters, k, K_p and X are defined differently for each reaction ($R1$) or ($R2$), consistent with the previous discussion. Here, $\varepsilon_{bed} = 0.36$ is the mean interstitial porosity of the bed, $v = 3.88$ m/s is the interstitial velocity, $A_s = 8.2 \times 10^{-5}$ m^2 is the circular cross-sectional area of the bed, K_p is the equilibrium constant, and $D = 8 \times 10^{-4}$ m^2 /s is the dispersion coefficient, which was calculated using Eq. 12 from Gunn[28] and verified with Levenspiel's Figure 13.17.[23] The mass transfer coefficients, $k_{g,CO}$ and k_{g,CO_2}, from the bulk gas to the surface of the particles, which appear in the rate constant, k, were calculated using the correlation of Wakao and Funazkri,[29] $Sh = 2.0 + 1.1Sc^{1/3}Re^{0.6}$. Hence, all the parameters were experimentally obtained with the exception of the mass transfer and dispersion coefficients. Furthermore, the effect of the dispersion coefficient was small due to the large Péclet number, $Pe = vL/D = 160$. The equations were discretised using an upwind finite difference scheme. The length of the bed was $L = 33$ mm and the number of grid points used was 100. Boundary conditions were chosen to be of the Danckwerts form and were expressed for the case of CO as: $v(c_{CO}(0) - c_{CO,in}) - D(\partial c_{CO}/\partial x)_{x=0} = 0$ and $(\partial c_{CO}/\partial x)_{x=L} = 0$ at the inlet and outlet, respectively.[30] Here, $c_{CO}(0)$ is the concentration of CO at the grid point at the inlet to the bed, whereas $c_{CO,in}$ is the specified inlet concentration, which for as 9 vol % fraction at 1023 K and 101 kPa gives $c_{CO,in} = 1$ mol/m^3. The inlet [CO_2] was also 1 mol/m^3. To prevent the model from producing negative amounts of, $Fe_{0.947}O$, an additional thermodynamic constraint was added: the reduction of Fe_3O_4 to $Fe_{0.947}O$ (R2) in a differential element was not permitted unless locally $P_{co_2}/P_{co} < 2.1$, which represents the experimental equilibrium constant.

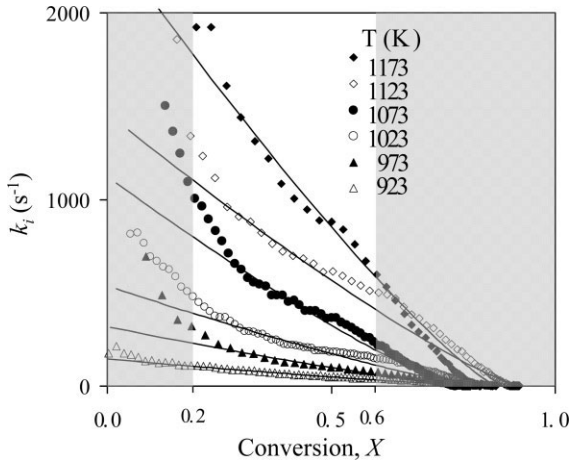

Figure 12. Plot of the rate term, k_i, versus conversion, X, for cycle 2 at various temperatures.

The rapid rise of k_i for $X < 0.2$ and the decrease of k_i toward zero with $X > 0.6$ is evident. Rates within the interval $0.2 < X < 0.6$ gave a best fit of $k_i = k_0(1 - X/0.8)^{1.2}$; this fit is indicated by the solid lines.

The packed bed, containing 5 g of Fe_2O_3 particles with $R \sim 180$ μm, was heated to 1023 K in a stream of air. The reactor was subsequently purged with N_2 for 500 s. At $t = 0$, the gas was suddenly changed from N_2 to a mixture of $N_2 + CO + CO_2$ (respectively, 82, 9, and 9 vol %), which from thermodynamics will reduce the Fe_2O_3 to $Fe_{0.947}O$, forming Fe_3O_4 as an intermediate. Reoxidation was performed with N_2+steam (respectively, 82 and 18 vol %) and N_2+air (respectively, 82 and 18 vol %). Figure 13 shows the concentrations of CO and CO_2 at the reactor outlet, $x = L$, as a function of time for the second reduction cycle. Initially, for 0 s $< t <$ 90 s, Figure 13 shows that the entering CO is fully converted to CO_2. In this interval, a front corresponding to the reduction of Fe_2O_3 to Fe_3O_4 in reaction (R1), propagates down the bed. The intrinsic kinetics are sufficiently fast to permit equilibrium to be reached, so that the ratio $[CO]/[CO_2] = 1/K_p \approx 0$. The relation between the residence time of the gas and the characteristic kinetic time constant also demonstrates that reactant gases have sufficient time to fully react, since $1/k < L/v$. The breakthrough of the front after $t \sim 95$ s is characterised by a rapid rise and fall in the concentrations of CO and CO_2, respectively. At this stage the Fe_2O_3 along the bed has been fully converted to Fe_3O_4; also $Fe_{0.947}O$ has appeared at the reactor inlet. The conversion of Fe_3O_4 to $Fe_{0.947}O$, which has already commenced at the beginning of the bed for $t < 95$ s, continues until $t \sim 410$ s. For $t > 200$ s, the curvature of the outlet concentrations is primarily governed by kinetics and the accuracy of the value of k for (R2) is demonstrated by the good agreement between the experimental and modeled concentration curves. For $t > 410$ s no more reaction occurs and the concentrations of CO and CO_2 in the outlet are equal to those at the inlet, i.e., 1 mol/m^3. The arrows in Figure 13 indicate the times when various metal oxide species were present above 5 mol% at the reactor outlet, i.e., in the final computational cell. The narrow overlap between the Fe_2O_3 and Fe_3O_4 lines indicates a sharp front, compared to the more gradual transition between Fe_3O_4 and $Fe_{0.947}O$.

The influence of the dispersion coefficient was also investigated by increasing and decreasing D in the range $D = 8 \times 10^{-3}$ m^2 /s to $D = 8 \times 10^{-5}$ m^2 /s. Figure 13 shows that altering D by two orders of magnitude does not influence the results.

Discussion

For the design of equipment to reduce Fe_2O_3 using CO with subsequent reoxidation, the long-term stability of the rate of reduction over many cycles is important. Figure 5 shows that the initial rate constant, k_0, for the reduction from Fe_2O_3 to Fe_3O_4 did not decrease, but remained constant over nine cycles.

For the rate constants in Figure 6, the ratios of the resistance of external mass transfer of CO to the resistance of intrinsic kinetics, i.e., the ratio of the sum of the first and third terms in Eq. 5 divided by the second term, was ~0.01 and ~0.15 at 723 K and 923 K, respectively, thus ensuring that the experimental rates were dominated by intrinsic kinetics. Figure 4b confirmed that the effectiveness factor was near unity at 823 K for particles with $R \approx 150 - 210$ μm. It was observed that the deduced activation energy was approximately halved when the particle size was increased, see Figure 6, suggesting that the effectiveness factor was unity for small particles and that the rate of reduction for the larger particles was controlled by intraparticle diffusion. For the initial rate constant, k_0, a pre-exponential factor of 2.4×10^7 s^{-1} and an activation energy of 75 $\pm$ 11 kJ/mol was obtained; both values were constant over repeated cycles. By comparison, Trushenski et al.[19] give 69.0 kJ/mol $< E <$ 100.0 kJ/mol and Tsay et al.[20] report $E = 114$ kJ/mol. These authors' values were obtained from experiments with significant mass-transfer resistance.

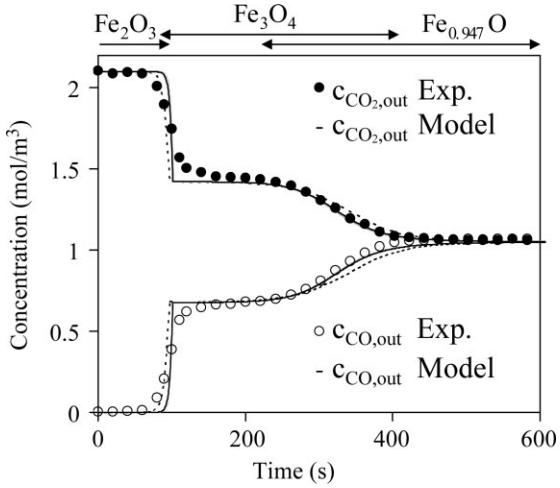

Figure 13. Comparison between the effluent concentration of CO and CO_2 as a function of time for experimental results (○,●) and model predictions (–,–), respectively, with $D = 8 \times 10^{-4}$ m^2/s.

Results with an increased dispersion of $D = 8 \times 10^{-3}$ m^2/s are shown by the dashed lines (- -, - -); results for a decreased dispersion of $D = 8 \times 10^{-5}$ m^2/s are similar to the original result (–,–).

Correctly incorporating a rate expression for a gas–solid reaction into a kinetic model can be difficult. Reaction rates are usually represented as the product of gaseous concentrations and a rate constant only; however, no reaction occurs unless the requisite solid species is present. Different strategies exist for determining whether a reaction is permitted to occur or not. Binary variables, indicating the presence of a solid, can be employed to switch reactions on or off. Alternatively, a more computationally benign, continuous function of solids' conversion can be used. Figure 7 shows that $f(X)$, giving the effect of conversion, X, is best represented by the function $(1 - X/0.8)^{0.4}$. Interpreting the exponent, $n = 0.4$, we find that terms of $(1 - X)^{1/3}$ and $(1 - X)^{1/2}$ are typical for theoretical rate expressions involving shrinking cores in spherical and cylindrical geometries, respectively, where the reaction is limited by intrinsic kinetics. However, in the current study, shrinking cores could not exist on the length scale of an individual particle, since the highly porous matrix allowed gas to diffuse across the entire cross-section. A shrinking core interpretation might, however, be applicable at the subparticle, e.g., grain, length scale.

For the transition from Fe_3O_4 to $Fe_{0.947}O$, K_p is of order unity and the influence of the back reaction, in suppressing the rate, permitted higher temperatures and reactant concentrations to be used in the determination of the rate constant, k_i. At a conversion of $X = 0.3$, the ratio of the resistance due to external mass transfer of CO and CO_2 to that of the chemical reaction, i.e., the central term in Eq. 5 divided by the sum of the two mass transfer terms in Eq. 5, was given as ~0.02 and ~0.17 at 923 K and 1173 K, respectively. The primary control of intrinsic kinetics was thus ensured and confirmed by effectiveness factors near unity for particles with $R \sim 180$ μm, see Figure 4. Unlike the transition from Fe_2O_3 to Fe_3O_4, Figure 10 showed that the rate constant decreased with cycle number. A decrease in rate implies that less iron oxide is converted to $Fe_{0.947}O$ in a given period of time and therefore less $Fe_{0.947}O$ is present to generate H_2. Efforts to produce particles for the repeated generation of H_2 should therefore focus on reaction (R2) and investigate how promoters or stabilizing agents could be used to prevent the decrease in rate over a number of cycles.

That the observed decrease in rate with cycle number (Figure 10) was a result of a decrease in the pre-exponential factor is demonstrated by the fact that the activation energy in Figure 11 showed only a slight decrease with cycle number: the average value of E was 94 ± 25 kJ/mol. Interpreting the activation energy and pre-exponential factor as a chemical barrier and a probability of a reactive collision occurring, respectively, these observations imply that the probability of reaction decreases with cycle number whilst the intrinsic chemical barrier remains constant. Physically, this interpretation suggests a morphological change with cycle number. A decrease in the reactive particle's surface area with cycle number could not, however, be verified with BET measurements, since the specific surface area of the fresh particles of 1 m^2/g was close to the accuracy limits of the analysis method. Figure 11 showed that E, found using the observed rate constant for particles which were one order of magnitude larger than those in the kinetic study, resulted in an apparent E half as large as that found in the kinetic study. Comparing $E = 94 \pm 25$ kJ/mol obtained here, Trushenski et al.[19] gives 64.4 kJ/mol $< E <$ 78.2 kJ/mol and Tsay et al.[20] report $E = 73.6$ kJ/mol. These authors' values were obtained from experiments with significant mass-transfer resistance.

The dependence of solids' conversion on k was more difficult to determine for the transition from Fe_3O_4 to $Fe_{0.947}O$. Uncertainty in the term, $(c_{CO,out} - c_{CO_2,out}/K_p)/r'$, meant that k could only be determined with reasonable accuracy for $0.2 < X < 0.6$. Figure 12 showed that $f(X)$ is best represented by $(1 - X/0.8)^{1.2}$. The term $(1–X)^a$ with $a = 1$ is typical for a uniform reaction over a porous sphere. Finally, it should be noted that reduction to Fe was not studied. Similar to a previous study[3] it was found that reduction to Fe was only possible for a single cycle, after which the particles were unreactive.

The rate constants were verified by investigating the consecutive reduction of Fe_2O_3 to $Fe_{0.947}O$ in a packed bed. Figure 13 showed good agreement between observed and predicted values of [CO] and [CO_2] in the effluent for the reduction of Fe_3O_4 to $Fe_{0.947}O$, i.e., for $t > 94$ s. The front, corresponding to the initial reduction from Fe_2O_3 to Fe_3O_4 shown at $t = 95$ s in Figure 13, was sharper in the model than in the experiment. Better agreement with the experimental observations could be achieved by incorporating the resistance to intraparticle diffusion through an effectiveness factor $\eta < 1$, which would slightly decrease k and smooth out the sharp step change. The model showed that the reduction of Fe_2O_3 to Fe_3O_4 occurred at a sharper front than the more gradual reduction of Fe_3O_4 to $Fe_{0.947}O$, see Figure 13. This observation is a direct result of the value of the rate constants, since k for (R1) is much greater than k for (R2) at a given temperature.

Conclusion

The repeated reduction of Fe_2O_3 to Fe_3O_4 and of Fe_3O_4 to $Fe_{0.947}O$ by CO and CO_2 mixtures was studied in a fluidised bed at 101 kPa and at temperatures of 723–973 K and 923–1173 K, respectively. The order of reaction for CO was found to be unity in both reduction reactions. The rate constant remained constant with cycle number for the transition from Fe_2O_3 to Fe_3O_4, but decreased for the transition from Fe_3O_4 and $Fe_{0.947}O$. The variation of the rate with solids' conversion and temperature was expressed as:

$$Fe_2O_3 \rightarrow Fe_3O_4:$$

$$r' = \frac{2.4 \times 10^7 \exp\left(\frac{-75000}{RT}\right)}{\rho_{Fe_2O_3}} \left(c_{CO} - \frac{c_{CO_2}}{K_p}\right) \left(1 - \frac{X}{0.8}\right)^{0.4} \quad (10)$$

$$Fe_3O_4 \rightarrow Fe_{0.947}O:$$

$$r' = \frac{4.3 \times 10^7 \exp\left(\frac{-94000}{RT}\right)}{\rho_{Fe_2O_3}} \left(c_{CO} - \frac{c_{CO_2}}{K_p}\right) \left(1 - \frac{X}{0.8}\right)^{1.2}, \quad (11)$$

where the pre-exponential factor in Eq. 11 is reported for cycle 2. The activation energies were verified by showing that for larger particles where intraparticle diffusion limits the rate, the observed activation energy approximately halves. The rate constants, determined in a fluidised bed, were used to

predict successfully the reduction of iron oxide in a packed bed.

Acknowledgments

Financial support from the following organizations is gratefully acknowledged: Engineering and Physical Sciences Research Council (EP/F027435/1); Gates Cambridge Trust.

Notation

a = index for curve fitting
A_s = reactor cross-sectional area (m^2)
A = pre-exponential factor (1/s)
b_1 = constant in Eq. 2 (mol/m^3)
Bi = Biot number = $hd_p/6\lambda_p$
c_1 = constant in Eq. 2 (mol/m^2)
c_{CO}, c_{CO_2} = concentration (mol/m^2)
$c_{CO,out}$, $c_{CO_2,out}$ = concentration at reactor outlet (mol/m^3)
$c_{CO,in}$, $c_{CO_2,in}$ = concentration at reactor inlet (mol/m^3)
$c_{CO,p}$, $c_{CO_2,p}$ = concentration in particulate phase (mol/m^3)
$c_{CO,s}$, $c_{CO_2,s}$ = concentration at particle surface (mol/m^3)
d_1 = constant in Eq. 2
d_{bed} = bed diameter (m)
d_p = particle diameter (m)
D = packed bed dispersion coefficient (m^2/s)
D_e = effective diffusivity (m^2/s)
$D_{e,CO}$, D_{e,CO_2} = effective diffusivity (m^2/s)
$D_{k,CO}$, D_{k,CO_2} = Knudsen diffusivity (m^2/s)
$D_{mix,CO}$, D_{mix,CO_2} = diffusivity CO and CO_2 in a gas mixture (m^2/s)
E = activation energy (J/mol)
h = heat transfer coefficient between reacting particle and bed (J/(m^2 s K))
H_0 = unfluidised bed height (m)
k = effective rate constant, including mass transfer effects (1/s)
k_i = intrinsic rate constant, chemical rate-controlled (1/s)
k_0 = initial value of k_i at $X = 0$, $t = 0$ (1/s)
$k_{g,CO}$, k_{g,CO_2} = external mass transfer coefficient for a particle (m/s)
K_p = equilibrium constant equal to p_{CO_2}/pCO
L = length of the packed bed (m)
m = number of experimental points
M_w = molecular weight (g/mol)
$n_{Fe_2O_3}$, $n_{Fe_2O_4}$ = moles of iron oxide per unit volume of bed (mol/m^3)
Nu = Nusselt number = hd_p/λ_g
Pe = Péclet number = vL/D
p_{CO}, p_{CO_2} = partial pressure (Pa)
r = radial position within particle (m)
r' = rate of reaction per unit mass of particle as Fe_2O_3 (mol/(s g))
R = external particle radius (m)
R = ideal gas constant (J/(mol K))
Re = Reynolds number = $\rho_g U d_p/\mu_g$
Re_p = particle Reynolds number = $\rho_g U_{mf} d_p/\mu_g \varepsilon_{mf}$
Sc = Schmidt number = $\mu_g/\rho_g D_{mix}$
Sh = Sherwood number = $k_g d_p/D_{mix}$
S_g = specific surface area (m^2/g)
t = time (s)
T = absolute temperature (K)
u_{CO} = variable equal to $c_{CO}\, r$ (mol/m^2)
U = superficial velocity of fluidising gas(m/s)
U_{mf} = value of U at incipient fluidization (m/s)
v = packed bed interstitial velocity (m/s)
W = mass of a single particle of Fe_2O_3 (g)
x = distance along packed bed (m)
X = conversion of solid reactant, $(n_{Fe_2O_3,t=0} - n_{Fe_2O_3})/n_{Fe_2O_3,t=0}$ or $\left(\frac{2}{3}n_{Fe_2O_3,t=0} - n_{Fe_3O_4}\right)/\left(\frac{2}{3}n_{Fe_2O_3,t=0}\right)$

Greek letters

ε = particle porosity
ε_{mf} = fluidised bed porosity at U_{mf}
ε_{bed} = packed bed porosity due to interstices
η = effectiveness factor = $3(\phi \coth \phi - 1)/\phi^2$
λ_g = thermal conductivity of the gas (J/(m s K))
λ_p = thermal conductivity of the porous particle (J/(m s K))
μ_g = viscosity of the gas (kg/(m s))
ϕ = Thiele modulus = $R[k_i/D_{e,CO} + k_i/(K_p D_{e,CO_2})]^{1/2}$
ρ_g = density of the gas (kg/m^3)
$\rho_{Fe_2O_3}$, $\rho_{Fe_3O_4}$ = initial particle density (particle mass/particle volume) (g/m^3)
τ_{CO}, τ_{CO_2} = mixing time constants (s)
τ = tortuosity

Literature Cited

1. IPCC. IPCC Climate Change 2007, Fourth Assessment Synthesis Report, 2007, Cambridge University Press, Cambridge.
2. v. Bogdandy L, Engell H-J. *The Reduction of Iron Ores*. Berlin: Springer-Verlag, 1971:19–30.
3. Bohn CD, Müller CM, Cleeton JP, Hayhurst AN, Davidson JF, Scott SA, Dennis JS. Production of very pure hydrogen with simultaneous capture of carbon dioxide using the redox reactions of iron oxides in packed beds. *Ind Eng Chem Res*. 2008;47:7623–7630.
4. Farrauto R, Hwang S, Shore L, Ruettinger W, Lampert J, Giroux T, Liu Y, Ilinisch O. New material needs for hydrocarbon fuel processing: Generating hydrogen for the PEM fuel cell. *Annu Rev Mater Res*. 2003;33:1–27.
5. Messerschmitt A. *Process of Producing Hydrogen*. U.S. Pat. 971,206. 1910.
6. Huebler J, Johnson JL, Schora FC, Tarman PB. *Production of Hydrogen via the Steam-Iron Process*. U.S. Pat. 3,442,620. 1969.
7. Reed HC, Berg CH. *Hydrogen Process*. U.S. Pat. 2,635,947. 1953.
8. Chuang SY, Dennis JS, Hayhurst AN, Scott SA. Development and performance of Cu-based oxygen carriers for chemical-looping combustion. *Combust Flame*. 2008;154:109–121.
9. Johansson M, Mattisson T, Lyngfelt A, Abad A. Using continuous and pulse experiments to compare two promising nickel-based oxygen carriers for use in chemical-looping technologies. *Fuel*. 2008; 87:988–1001.
10. Barin I, Knacke O. *Thermochemical Properties of Inorganic Substances*. Berlin: Springer-Verlag; 1973.
11. McBride BJ, Zehe MJ, Gordon S. NASA *Glenn Coefficients for Calculating Thermodynamic Properties of Individual Species*. NASA Report: TP-2002–211556. 2002.
12. Omori Y, editor. *Blast Furnace Phenomena and Modelling*. London: Elsevier, 1987:121–135.
13. McKewan WM. Kinetics of iron ore reduction. *Trans Metall Soc AIME*. 1958;212:791–793.
14. McKewan WM. Reduction kinetics of hematite in hydrogen-water vapor-nitrogen mixtures. *Trans Metall Soc AIME*. 1962;224:2–5.
15. Spitzer RH, Manning FS, Philbrook WO. Generalized model for the gaseous, topochemical reduction of porous hematite spheres. *Trans Metall Soc AIME*. 1966;236:1715–1724.
16. Murayama T, Ono Y, Kawai Y. Step-wise reduction of hematite pellets with CO–CO_2 gas mixtures. *Tetsu-to-Hagané*. 1977;63:1099–1107.
17. Szekely J, Evans JW. A structural model for gas-solid reactions with a moving boundary. *Chem Eng Sci* 1970;25:1091–1107.
18. Valipour MS, Saboohi Y. Modeling of multiple noncatalytic gas-solid reactions in a moving bed of porous pellets based on finite volume method. *Heat Mass Transfer*. 2007;43:881–894.
19. Trushenski SP, Li K, Philbrook WO. Non-topochemical reduction of iron oxides. *Metall Trans*. 1974;5:1149–1158.
20. Tsay QT, Ray WH, Szekely J. The modelling of hematite reduction with hydrogen plus carbon monoxide mixtures. *AIChE J*. 1976;22:1064–1072.
21. Wen CJ, Yu YH. A generalized method for predicting the minimum fluidization velocity. *AIChE J*. 1966;12:610–612.
22. Smith NL, Amundson NR. Intraparticle diffusion in catalytic heterogeneous systems. *Ind Eng Chem Res* 1951;43:2156–2167.
23. Levenspiel O. *Chemical Reactor Engineering*, *3rd ed*. John Wiley & Sons, New York; 1999:385–391.

24. Davidson JF, Harrison D. *Fluidised Particles*. Cambridge: Cambridge University Press, 1963:97–106.
25. La Nauze RD. Fundamentals of coal combustion in fluidised beds. *Chem Eng Res Des*. 1985;63:3–33.
26. Hirschfelder JO, Curtiss CF, Bird RB. *Molecular Theory of Gases and Liquids*. New York: John Wiley & Sons, 1954.
27. Satterfield CN. *Heterogeneous Catalysis in Practice*. London: McGraw-Hill, 1980.
28. Gunn DJ. Mixing in packed and fluidised beds. *Chem Eng*. 1968; 214:CE153–CE172.
29. Wakao N, Funazkri T. Effect of fluid dispersion coefficients on particle-to-fluid mass transfer coefficients in packed beds. *Chem Eng Sci*. 1978;33:1375–1384.
30. Beers KJ. *Numerical Methods for Chemical Engineering*. Cambridge: Cambridge University Press, 2007:279–282.

Manuscript received Apr. 6, 2009, and revision received Aug. 28, 2009.